# Characterization of AGV Localization System in Industrial Scenarios Using UWB Technology

Paula Verde, Javier Díez-González, Rubén Álvarez, and Hilde Perez

***Abstract*— Automatic guided vehicles (AGVs) are indispensable elements for the advancement of Industry 4.0 and the digital transformation of factories. These industrial vehicles use embedded intelligence to orient themselves and plan their routes in the short term with the aim of achieving a collaborative, safe, and efficient environment, increasing the competitiveness of industrial plants. However, AGVs still present some challenges that do not allow the full deployment of these vehicles for precision industrial tasks. For this reason, in this article, we propose a localization system to enhance the position determination of AGVs in the industrial plant. This system is based on a wireless ad hoc network that modulates the localization signal through ultra-wideband (UWB) technology to take advantage of the very short duration of the emitted pulses granting robustness against the multipath and non-line-of-sight (NLOS) negative effects typical of industrial environments. In addition, we optimize the location of the architecture sensors through a metaheuristic algorithm (MA-VND-Chains) that requires the definition of the system localization uncertainties given a particular sensor arrangement. For this purpose, we introduce in this article the most complete characterization of the uncertainties of the time difference of arrival (TDOA) localization architecture based on noise, clock, and multipath effects. This allows us to finally obtain localization errors up to six centimeters, thus attaining the required accuracy for AGVs to address high-demanded accuracy applications within the industrial plant.**

***Index Terms*— Automatic guided vehicle (AGV), Cramér-Rao bounds (CRBs), indoor localization, local positioning systems (LPSs), metaheuristics, multipath, time difference of arrival (TDOA), ultra wide-band (UWB).**

## I. Introduction

AUTOMATED guided vehicles (AGVs) are supposing a revolution for the internal automated transportation of goods within the digitized industry [1]. By means of embedded intelligence and the connectivity currently incorporated into them, AGVs achieve huge operability. These bases introduce AGVs in a collaborative industrial environment where their coordination with other AGVs and different industrial devices enables the addressing of complex industrial tasks [2].

However, the irruption of AGVs in industry still presents some remarkable challenges to fully deploy the advantages of these vehicles: the communication and coordination among different AGVs in a fleet, the generation of efficient trajectories in dynamic environments, their integration in industrial internet platforms, or reaching the adequate accuracy in indoor navigation for addressing precision applications [3].

Regarding their precision navigation, indoor AGVs localization is addressed through inertial, visual, or ranging procedures [4]. One of the technologies achieving very accurate results up to 5–10 cm of error bound in indoor spaces is the ultra-wideband (UWB) technology.

UWB takes advantage of the very short duration of the emitted pulses granting robustness against multipath interference which is critical for industrial saturated environments [5]. UWB indoor localization technology can modulate the localization signals of radioelectric local positioning systems (LPSs) which are finally employed to determine the target location in indoor spaces [6].

LPSs are deployments of wireless sensor networks (WSNs) that particularly adapt to the characteristics of the scenario of application [7]. This particular adaptation allows the arrangement of accurate and reliable localization systems in harsh environments (e.g., global navigation satellite systems (GNSSs) denied spaces or scenarios with high obstacles density).

The benefits of LPS are especially attracting the research interest in indoor environments since traditional GNSS signals significantly degrade when facing building walls [8]. In addition, other classical GNSS error sources (e.g., non-line-of-sight (NLOS) links among the system devices [9] or multipath appearance [10]) are severely mitigated in indoor spaces with a significant number of obstacles such as people, furniture, or industrial equipment.

LPS address these GNSS limitations through systems classified depending on the physical property measured for determining the target location: time, frequency, angle, phase, power, or combinations of them [11].

Among them, time-based systems stand out for indoor spaces since they present the best trade-off among robustness, reliability, easy-to-implement hardware architectures, accuracy, and costs [12]. Three main time-based architectures are considered in the literature: time of arrival (TOA), time difference of arrival (TDOA), and asynchronous TDOA (A-TDOA). They generate spherical, hyperbolic, or elliptic localization systems, respectively [13].

TDOA systems are especially suitable for indoor applications since these systems stand out in NLOS channel-dominant conditions [14] or potential sensor failure situations [15].

Manuscript received 12 January 2023; revised 14 June 2023; accepted 25 June 2023. Date of publication 19 July 2023; date of current version 3 August 2023. This work was supported in part by the Spanish Ministry of Science and Innovation Project under Grant PID2019-108277GB-C21/AEI/10.13039/501100011033 and in part by the University of León. The Associate Editor coordinating the review process was Dr. Yong Yan. *(Corresponding author: Javier Díez-González.)*

The authors are with the Department of Mechanical, Computer and Aerospace Engineering, Universidad de León, 24071 León, Spain (e-mail: jdieg@unileon.es).

Digital Object Identifier 10.1109/TIM.2023.3296817

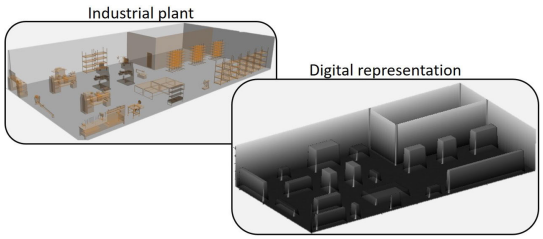


Fig. 1. Representation of the industrial plant of this article (left), and its digital representation for the sensors' location optimization addressed to improve the AGVs localization system (right).

These are typical factory conditions where AGVs are deployed.

Therefore, we propose in this article a UWB TDOA localization system for allowing the precise localization of AGVs in industrial indoor environments such as the industrial plant composed of machines and industrial devices presented in Fig. 1. This scenario, where AGVs are used for internal transportation, represents typical factory conditions where NLOS and multipath are critical factors in attaining robust and accurate localization.

The performance of the proposed LPS is highly determined by the location of the sensor nodes of the architecture. This enables reducing the errors produced by NLOS propagation links and multipath interference effects. To achieve this purpose, an accurate modeling and measurement of the orography is necessary, thus shaping the surface of the deployment region for finding the optimal location for the sensor nodes. In the literature, this is known as the node location problem (NLP) [16].

A high number of potential locations for the sensors analyzed increases the computational complexity of the NLP, which has been assigned as NP-Hard both in coverage and accuracy in the localization field [17]. This implies that most of the literature approaches for the NLP are tackled through metaheuristic algorithms (e.g., genetic [18], memetic [19], or bio-inspired algorithms [20], [21], [22]).

However, the efficiency of these methods depends on the adjustment of these algorithms to tackle the specific problem addressed. For this reason, we propose in this article the employment of the MA-VND-Chains algorithm [23] that we recently proposed to address the NLP optimization considering the particular characteristics of this problem in LOS/NLOS environments.

A fitness function to measure the quality of the sensor distribution in space is required for the optimization. In the localization field, it is common to employ the Cramér-Rao bounds (CRBs) to compute the minimum achievable error of a particular sensor arrangement regardless of the localization algorithm used to determine the target location [24].

Traditional CRB characterizations have considered positioning signal path degradation in LOS environments [25], [26]. We recently added to this CRB characterization the consideration of the signal path degradation in LOS/NLOS environments through the development of a ray-tracing algorithm [10] that we completed with the analysis of the clock errors during the time measurements in [27].

This error characterization was later proven in actual environments, showing that our approach better described the error bounds than traditional CRB characterizations in an actual UWB TDOA localization system [28]. However, there is still a difference between the actual localization errors and our proposed CRB which may be due to multipath interference.

For this reason, in this article, we complete our CRB model by adding the error effects of multipath interference to the clock and signal path losses in an indoor UWB TDOA positioning system. The main objective is to optimize the deployment of sensors of the LPS within an industrial plant using the proposed MA-VND-Chains optimization algorithm. By employing the improved CRB model as the fitness function, the algorithm aims to minimize localization errors across the entire coverage region necessary for AGVs navigation. The proposed approach significantly reduces overall localization errors, enabling AGVs to perform precise tasks with improved accuracy and enhancing their navigation capabilities in industrial environments.

Therefore, the main contributions of this article can be summarized as follows.

1) The proposal of a combined UWB TDOA localization system to enhance the signal quality and precision navigation of AGVs in industrial plants.
2) The most complete characterization in the current literature of the error bounds of the TDOA architecture in indoor environments considering noise, clock, and multipath uncertainties.
3) The definition of a novel adaptive encoding and decoding of the NLP through the development of the polyhedron formed by the building walls of the scenario of application. This exclusively ensures the generation of valid individuals for the location of the TDOA architecture sensors.
4) The proposal of an optimal localization system through the utilization of the MA-VND-Chains algorithm, specifically tailored to address obstacles and indoor conditions.
5) The minimization of the localization system error in the entire navigation area of the AGVs in the industrial plant.

The remainder of the article is organized as follows: we revise the UWB technology with its benefits for indoor localization in Section II; the novel CRB characterization considering signal path losses, clock uncertainties, and multipath is proposed in Section III; Section IV presents the specifications of the industrial scenario of application of the UWB TDOA system proposed together with the mathematical model of the problem addressed; the MA-VND-Chains algorithm used for the NLP optimization is shown in Section V while Sections VI and VII present the results achieved and the conclusions of the article, respectively.

## II. Related Works of UWB Indoor Localization

The digital transformation implied by Industry 4.0 makes it possible to advance in the communication and cooperation of collaborative agents such as AGVs and employees,

achieving more advanced and optimized production systems. However, as new services are added, industrial communication networks have to increase their capacity to exchange data and transmit them at low latency. Many of these services, such as target localization, require of wireless technology, which has led authors such as Kunst et al. [29] to develop techniques to improve their communications. In addition, electromagnetic interference (EMI) produced by electronic devices operating nearby [30] such as industrial machines or phones, increases electromagnetic fields, promoting the appearance of noise incorporated into the communications channels. The EMI effect is a serious problem of digital systems [31], which has forced the selection of resistant technologies [32].

The transmissions of UWB are composed of energy pulses modulated in the order of picoseconds where aspects such as amplitude, polarization, or phase are varied to encode the information. These signals separated by at least one pulsewidth duration maintain their individuality without overlapping [33]. The short pulses and large bandwidth help reduce the effect of severe multipath interference, as those unwanted paths are exhausted making it easier to receive the signal at the receiver [34].

Industrial scenarios are composed of objects, materials [35], and architectural elements that, in addition to generating multiple paths, attenuate the signals trying to pass through them. The frequency used in the UWB signal coding allows for attenuating the material penetration losses, favoring the signal strength during communication [36]. The short pulses, together with the radio energy dispersion techniques it applies, spread their energy over a wide frequency range with a low-power spectral density. This generates a high bandwidth that allows high data throughput during communication and a longer lifetime in portable systems. In addition, the existence of external noise and devices does not significantly affect the technology due to its high bandwidth and signal modulation.

In the literature, there are many studies that examine the advantages of UWB technology. For example, Machaj et al. [37] conduct a pedestrian localization study in indoor environments (i.e., offices and gyms) and highlight the very accurate localization of UWB concerning WiFi and Zigbee technologies. However, the industrial scenarios are more complex compared to the consumer indoor scenarios [35]. Therefore, as proposed by Schroeer [35], industrial UWB solutions have to be more accurate and reliable since inaccurate information can generate pernicious decisions. For this reason Krishnan et al. [38] developed machine learning (ML) algorithms to minimize the impact of NLOS conditions, Barbieri et al. [39] implemented a Bayesian filtering method to mitigate object motion dynamics and visibility conditions and Yang [40] generated an NLOS mitigation model based on the sparse pseudo-input Gaussian process (SPGP).

Most of the current techniques for mitigating adverse conditions for a TDOA architecture with indoor UWB technology focus on acting on the signals when the architecture is already deployed. This is the case of authors such as Cheng and Zhou [41] who conduct a study to test which methodology presents a lower error in localization by deploying the sensors at the corners of the study scenario, Liu et al. [42] which improve the signal conditions and reduce the impact of NLOS conditions in real time through a target tracking algorithm, and Bocquet et al. [43] which focused on techniques on UWB technology that improve localization results.

However, the analysis of the location of the nodes allows to reduce to a great extent the NLOS conditions and thus minimize the CRB. For instance, Pan et al. [44] developed a node placement technique where decimeter-level target location accuracy is attained. Nevertheless, the CRB used by these authors is incomplete [28] as it only takes into account path losses.

Thus, considering the literature analyzed, we perform in this article a complete preliminary study on the deployment of an ad hoc UWB localization system based on the orography of the scenario, signal degradation (i.e., path loss and multipath errors) and clock errors to determine an optimized WSN deployment. The analysis proposed allows us to reduce the NLOS degradation of the localization signal, the minimization of the multipath errors, and ultimately reduce the localization error in the entire navigation area of the AGVs.

For this purpose, we collect in Table I the values used by UWB applications in WSN indoor localization obtained from the analyzed literature which are later used during the NLP optimization performed in this article for mitigating NLOS and multipath effects in the localization signal.

TABLE I

BROADBAND CONFIGURATION MEASUREMENTS [45], [46]

| Parameter | Value |
|---|---|
| Frequency | 3.9 GHz |
| Transmitted bandwith | $\geq$500MHz |
| Power transmitted | 10.4 dBm |
| Attenna Gain | 3 dBi |
| Sensitivity | -100 dBm |

These features constituting the UWB signal enable centimeter-level accuracies in target localization [47]. This is a critical task for AGVs as this reachable accuracy enables their collaboration with other cyber-physical systems (CS) within the Industry 4.0 paradigm [2]. To achieve this goal, it is necessary to know the lower bound of the accuracy estimation on the signal delay. This value known as CRB allows us to know an estimation of the TDOA accuracy that can be obtained in a particular location of the scenario as presented in Section III.

## III. CRB CHARACTERIZATION FOR A UWB TDOA ARCHITECTURE CONSIDERING NOISE, CLOCK, AND MULTIPATH ERRORS

Signal propagation and positioning signal treatment produce uncertainties that degrade the localization system in terms of accuracy and stability. These uncertainties, resulting in inaccurate physical measurements, are introduced into the localization algorithms generating errors in the position estimation [41]. For this reason, different localization algorithms

are proposed in the literature for reducing the position calculation uncertainties [41], [48], [49].

However, the error bounds of these algorithms are limited by obtaining the best combination of the imperfect time measurements received in the architecture sensor nodes. In this sense, the minimum achievable error in a particular target sensor (TS) location can be obtained through the CRBs [49].

The CRB is based on the inverse of the fisher information matrix (FIM) and allows the finding the minimum variance of an unbiased estimator of a deterministic unknown parameter [50]. When it is applied to the TS coordinates, the CRB determines the minimum variance in the position calculation given a determined sensor arrangement in space.

Generally, the CRB has been used to characterize localization accuracy losses when the positioning signal is propagated from the TS to the architecture sensor nodes. The generated noise in the communications channel during transmission has been traditionally modeled through a white Gaussian noise distribution [26] that can be included in the definition of a generic matrix form of the FIM introduced by Kaune et al. [24]

$$\mathrm{FIM}_{mn} = \left(\frac{\delta h(\mathrm{TS})}{\delta \mathrm{TS}_m}\right)^{\mathrm{T}} \boldsymbol{R}^{-1}(\mathbf{TS})\left(\frac{\delta h(\mathrm{TS})}{\delta \mathrm{TS}_n}\right) + \frac{1}{2}\mathrm{tr}\left\{\boldsymbol{R}^{-1}(\mathbf{TS})\left(\frac{\delta R(\mathrm{TS})}{\delta \mathrm{TS}_m}\right)\boldsymbol{R}^{-1}(\mathbf{TS})\left(\frac{\delta R(\mathrm{TS})}{\delta \mathrm{TS}_n}\right)\right\} \tag{1}$$

where $m$ and $n$ are the TS coordinates analyzed for the FIM element ($\mathrm{FIM}_{mn}$), $\mathbf{h}(\mathbf{TS})$ is the vector containing the spatial propagation of the positioning signal in the architecture analyzed and $\mathbf{R}(\mathbf{TS})$ is the covariance matrix of the system.

Particularizing for the TDOA architecture used in this article, the vector $\mathbf{h}(\mathbf{TS})$ can be obtained as follows:

$$h_{\mathrm{TDOA}_i} = \|\mathrm{TS} - \mathrm{CS}_i\| - \left\|\mathrm{TS} - \mathrm{CS}_j\right\|, \quad i = 1, \ldots, N_{\mathrm{CS}}; \quad j = 1, \ldots, N_{\mathrm{CS}}; \; i \neq j \tag{2}$$

where CS are the coordinator sensors in which time measurements are collected for a particular TDOA architecture hyperboloid of potential TS locations [51]; $N_{\mathrm{CS}}$ is the number of CS with effective coverage in a determined TS location and $i$, $j$ represent the two different sensors involved in the TDOA time measurement analyzed.

The definition of the covariance matrix $\mathbf{R}(\mathbf{TS})$ allows a complete characterization of the system uncertainties. Most of the recent literature error models are based on the definition of the propagation uncertainties in a heteroscedastic noise consideration, since the signal travel from the TS to the CS may differ considerably among sensors [52], [53].

For this reason, we introduced in [10] and [54], a characterization of the system uncertainties in LOS/NLOS environments considering heteroscedastic noises. Since Sahinoglu et al. [55] proved that the TDOA architecture time measurements are correlated, the nondiagonal terms of the covariance matrix are distinct to zero.

Therefore, considering these conditions, we introduced a model for estimating the noise uncertainties in the covariance matrix of the TDOA architecture through a log-normal path loss model, especially indicated for modeling the decay of the positioning signal in indoor environments, due to the noise produced in the communications channel [56]

$$\sigma^2_{\mathrm{TDOA(noise)}_{ij}} = \frac{c^2}{B^2\left(\frac{P_T}{P_N}\right)}\mathrm{PL}(d_0) \times \left[\left(\frac{d_{i_{\mathrm{LOS}}}}{d_0}\right)_{\mathrm{CSi}} + \left(\frac{d_{i_{\mathrm{NLOS}}}}{d_0}\right)_{\mathrm{CSi}}^{\frac{n_{\mathrm{NLOS}}}{n_{\mathrm{LOS}}}} + \left(\frac{d_{j_{\mathrm{LOS}}}}{d_0}\right)_{\mathrm{CSj}} + \left(\frac{d_{j_{\mathrm{NLOS}}}}{d_0}\right)_{\mathrm{CSj}}^{\frac{n_{\mathrm{NLOS}}}{n_{\mathrm{LOS}}}}\right]^{n_{\mathrm{LOS}}} \tag{3}$$

$$d_{i_{\mathrm{LOS}}} = \|\mathrm{TS} - \mathrm{CS}_i\|_{\mathrm{LOS}} \tag{4}$$

$$d_{i_{\mathrm{NLOS}}} = \|\mathrm{TS} - \mathrm{CS}_i\|_{\mathrm{NLOS}} \tag{5}$$

$$d_{j_{\mathrm{LOS}}} = \left\|\mathrm{TS} - \mathrm{CS}_j\right\|_{\mathrm{LOS}} \tag{6}$$

$$d_{j_{\mathrm{NLOS}}} = \left\|\mathrm{TS} - \mathrm{CS}_j\right\|_{\mathrm{NLOS}} \tag{7}$$

where $c$ is the speed of the radioelectric waves in m/s; $B$ is the signal bandwidth in Hz; $P_T$ is the transmission power in W; $P_n$ is the mean noise level calculated through the Johnson–Nyquist equation, $\mathrm{PL}(d_0)$ is the path-loss at the reference distance ($d_0$) which in indoor UWB environments is usually fixed in 1 m [57]; $d_{i_{\mathrm{LOS}}}$, $d_{i_{\mathrm{NLOS}}}$, $d_{j_{\mathrm{LOS}}}$, and $d_{j_{\mathrm{NLOS}}}$ are the LOS/NLOS distances covered by the positioning signal to the $\mathrm{CS}_i$ and $\mathrm{CS}_j$, respectively, which are determined through the ray-tracing algorithm introduced in [10], and $n_{\mathrm{LOS}}$ and $n_{\mathrm{NLOS}}$ are the path-loss exponents in LOS/NLOS propagations of the positioning signal in indoor environments for the log-normal model considered.

Subsequently, we improved the error characterization of TDOA architectures through the consideration of clock uncertainties during the time measurements. Since the measurement process is independent from the propagation of the positioning signal, we proposed in [27] a combined noise and clock CRB characterization considering the independence of the variances generated by noise and clock uncertainties.

Specifically, our clock error model characterizes the uncertainties considering the initial time-offset ($U$) and the clock drift ($\eta$) as in Zhou et al. [58], adding the truncation effectuated due to the clock resolution ($\mathrm{floor}_{\mathrm{TR}}$). In addition, the stochastic nature of the time measurements cannot be introduced into a fitness function of a metaheuristic technique. This would promote instabilities during the posterior NLP optimization process. Thus, we perform a Monte Carlo simulation in which we determine the expected value for the clock uncertainties.

Therefore, the clock error characterization can be defined as follows:

$$\sigma^2_{\mathrm{TDOA(clock)}_{ij}} = \frac{1}{n_s}\sum_{k=1}^{n_s}\left\{|T_i - \mathrm{floor}_{\mathrm{TR}}(T_i + U_i - U_0 + T_0(\eta_i - \eta_0) + T_i\eta_i)|c^2\right\} + \frac{1}{n_s}\sum_{k=1}^{n_s}\left\{\left|T_j - \mathrm{floor}_{\mathrm{TR}}\left(T_j + U_j - U_0 + T_0\left(\eta_j - \eta_0\right) + T_j\eta_j\right)\right|c^2\right\} \tag{8}$$

where $n_S$ is the number of the Monte Carlo simulations performed to determine the expected value of the variance of

the clock uncertainties [27]; $T_i$ and $T_j$ are the ideal times of the positioning signals emitted from the TS and received in the $CS_i$ and $CS_j$, respectively; $U_i$, $U_j$, and $U_0$ are the initial-time offsets of the $CS_i$, $CS_j$, and TS clocks involved in the TDOA time measurement analyzed; $T_0$ is the ideal time lapse between the last synchronization of the architecture clocks and the emission of the positioning signal by the TS; $\eta_i$, $\eta_j$, and $\eta_0$ are the clock drifts of the $CS_i$ and $CS_j$ and the TS clocks, respectively.

This characterization of the CRB considering clock and noise uncertainties in TDOA architectures as proposed in [12] was initially discussed in the literature considering these two factors, being later on proven under an actual UWB TDOA localization system [28], demonstrating their superior performance to traditional literature approaches mostly based exclusively on noise uncertainties.

However, actual experiments showed a difference between the localization actual errors and the determined error bounds of our previously proposed CRB characterization. Thus, other error sources should be considered to try to further approximate the localization uncertainties. Among other potential uncertainties, multipath effects are especially relevant in industrial indoor environments due to the presence of multiple obstacles, machinery, and operators in the factory.

Consequently, we propose in this article to complete our CRB model considering the multipath error source. To include the multipath effects on the localization error, we assume the independence of the multipath error with regard to the noise uncertainties as presented in Wang et al. [59] for an indoor UWB TDOA localization system. Thus, as our previous assumption considered noise and clock uncertainties as independent, we can consider that the three error sources (i.e., noise, clock, and multipath) can be modeled separately.

For the characterization of the multipath uncertainties, we use the well-known statistical model for indoor multipath propagation by Saleh and Valenzuela [60]. We use it to characterize the multipath uncertainties in the two signal paths involved to compute a TDOA measurement, thus defining the multipath error variance as follows:

$$\sigma^2_{\text{TDOA(multipath)}_{ij}} = \bar{G}_i \log(1+d_i) + \bar{G}_j \log\left(1+d_j\right) \tag{9}$$

$$\bar{G}_i = G(d_0)\left[\left(\frac{d_{i_{\text{LOS}}}}{d_0}\right) + \left(\frac{d_{i_{\text{NLOS}}}}{d_0}\right)^{\frac{n_{\text{NLOS}}}{n_{\text{LOS}}}}\right]^{-n_{\text{LOS}}} \tag{10}$$

$$\bar{G}_j = G(d_0)\left[\left(\frac{d_{j_{\text{LOS}}}}{d_0}\right) + \left(\frac{d_{j_{\text{NLOS}}}}{d_0}\right)^{\frac{n_{\text{NLOS}}}{n_{\text{LOS}}}}\right]^{-n_{\text{LOS}}} \tag{11}$$

$$G(d_0) = \left(\frac{G_T G_R \lambda_0^2}{16\pi^2 d_0^2}\right) \tag{12}$$

where $\bar{G}_t$ and $\bar{G}_j$ represent the average multipath power gain in the positioning signal paths $i$ and $j$; $d_i$ and $d_j$ are the total distances covered for the positioning signal in the two trajectories; $G(d_0)$ is the multipath power gain at the reference distance (i.e., 1 m in indoor environments [60]); $G_T$ and $G_R$ are the gains of the transmitting (i.e., AGV onboard antenna) and receiving antennas (i.e., architecture sensor antennas); and $\lambda_0$ is the wavelength of the localization UWB signal.

**Algorithm 1** Calculation of the CRB ($TS$, $Frequency$, $G_0$, $G_T$, $G_R$, $n_{LOS}$, $n_{NLOS}$, $RMSE_{ref}$, $K_{OA}$, $K_{TLE}$, $SNR_{min}$, $\eta_{clock}$, $floor_{TR}$)

```
for TS in K_TLE do
    for Sensor in Individual do
        φ_link_sensor ← Ray-Tracing method (K_OA, TS, Sensor);
        Signal ← SNR calculation (SNR_min, φ_link_sensor, n_LOS, n_NLOS);
        Sensors_avb add (Sensor) when Signal > SNR_min;
    end
    Sensors_m, Time_m, CS ← Calculation of effective measurements (Sensors_avb, φ_link)
    for m in Time_m do
        for Sensor in Sensors_m do
            σ²_time(m) ← Clock Errors (TS, Sensor, η_clock, floor_TR);
            σ²_noise(m) ← Noise Calculation (Sensor, φ_link, TS, n_LOS, n_NLOS, K_OA);
            σ²_multipath(m) ← Multipath Determination (Sensor, TS, Frequency, G_0, G_T, G_R, n_LOS, n_NLOS, K_OA);
        end
        R(TS)_m ← Determination of covariances matrix(σ²_time(m), σ²_noise(m), σ²_multipath(m), TS);
        for coord in (x, y, z) do
            ι_m(coord) = δh(TS)/δTS(coord) ← Calculation of the derivatives of the signal path (Sensors_m, TS, φ_link, n_LOS, n_NLOS);
            τ_m(coord) = δR(TS)/δTS(coord) ← Calculation of the derivatives of the R(TS) matrix (Sensors_m, TS, φ_link, n_LOS, n_NLOS, G_T, G_R, G_0, η_clock, floor_TR);
        end
    end
    FIM (TS) ← FIM (R(TS), ι, τ);
    RMSE(TS) ← Square root of the trace of the inverse of FIM;
end
```

Once characterized the noise, clock, and multipath uncertainties, the justified assumption of independence among them allows the construction of the **R**(**TS**) through the variances/covariances of the system as follows:

$$\sigma^2_{\text{TDOA}_{ij}} = \sigma^2_{\text{TDOA(noise)}_{ij}} + \sigma^2_{\text{TDOA(clock)}_{ij}} + \sigma^2_{\text{TDOA(multipath)}_{ij}}. \tag{13}$$

Finally, the construction of the whole **FIM** introduced in [24] through the error characterization of this article allows the definition of the root mean-squared error (RMSE) in the position calculation in a particular TS location (i.e., AGV localization) with the UWB TDOA architecture arrangement analyzed. This value can be directly obtained through the inverse of the **FIM**(**J**) with the following calculation [61], [62]:

$$\text{RMSE}(\text{AGV}_i) = \sqrt{\text{trace}(\mathbf{J})} \tag{14}$$

where RMSE ($\text{AGV}_i$) represents the RMSE in a particular AGV location $i$. The reduction of the RMSE in the whole area of coverage (i.e., the space for AGVs navigation in the factory) allows the attainment of competitive LPS sensor distributions in space which permits the precision operation of AGVs in the industrial plant.

To clarify the previously detailed equations and to indicate the signal characteristics used at each point of the TLE for the TDOA architecture, the CRB evaluation procedure is described in the following pseudocode.

The method starts by assessing the yield of each node of the TDOA LPS at every potential location for the indoor navigation of an AGV. The available sensors, $\text{Sensors}_{\text{avb}}$, are determined based on their received SNR evaluated through the ray-tracing algorithm introduced in [10] through the determination of the LOS/NLOS paths of the positioning signals with all the scenario obstacles, $K_{\text{OA}}$. The sensors are then grouped in pairs, named $\text{Sensors}_m$, which perform the TDOA time difference measurements, $\text{Time}_m$.

Subsequently, for each time measurement of each individual sensor, the algorithm calculates the time, noise, and multipath uncertainties [i.e., $\sigma^2_{\text{time}}(m)$, $\sigma^2_{\text{noise}}(m)$, and $\sigma^2_{\text{multipath}}(m)$] for all time measurements referred to the sensors with effective coverage through (3)–(12). From these measured uncertainties, the algorithm computes the covariances matrix $R(\text{TS})$ for the measurement row $m$.

Moreover, an analysis of the derivatives for the three Cartesian coordinates is performed for the traversed signal paths, and the attained covariances matrix, thus obtaining $\iota_m(\text{coord})$ and $\tau_m(\text{coord})$, respectively, for each measurement. All this information is required to build the FIM through (1).

Finally, the execution of (14) allows the calculation of the minimal error of the TDOA architecture in the analyzed TS location. This process must be repeated in the entire coverage region, $K_{\text{TLE}}$, to calculate the fitness function of the NLP optimization of this article through (30), which is addressed in Section IV.

## IV. Specification of the Proposed Scenario

With the aim to calculate the RMSE obtained by the sensors belonging to the TDOA architecture, it is necessary to characterize a 3-D scenario that allows the reproduction of the conditions of a real factory through a combination of the target location environment (TLE), node location environment (NLE) and obstacle areas (Oas) regions. This strategy has been previously used to represent rural [51] and urban scenarios [12] with the same objective.

In the rural scenario, there are uneven ground slopes, larger distances to be covered, and diverse topography for the NLE and the TLE environments (e.g., natural landscape as mountains). In contrast, the urban scenario features elevated structures (e.g., signals, traffic lights, or buildings) as part of the NLE, that can allow optimizing the signal reception and minimizing interference. In addition, TLE tends to be more constantly distributed. In this article, we present for the first time the characterization of an indoor scenario with its particularities.

TLE delimits every potential location where targets can be placed within the industrial plant (i.e., the area of operation of AGVs including transit, loading and unloading of materials, and collaboration with other machinery or employees). Therefore, the transit and operation areas for workers are also enabled for AGVs to facilitate cooperation between both collectives. The height of this region is bounded by a lower and upper limit to be able to evaluate AGVs of different sizes, thus, as shown in the results section, the same positioning architecture allows positioning targets from 30 cm in height up to 2 m with a variation of the localization accuracy of less than 6%.

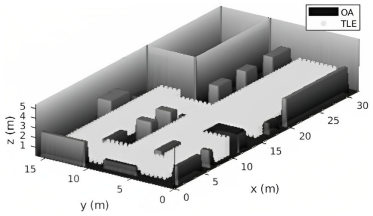


Fig. 2. Representation of the TLE and OA regions that compose the scenario.

TABLE II
Parameters That Define the Regions That Constitute the Scenario

| | Resolution (x,y,z) | Number of points | Height restrictions |
|---|---|---|---|
| NLE | [0.13, 0.13, 0.07] m | 65536 | $1\,\text{m} \leq h \leq 5.3\,\text{m}$ |
| TLE | [0.5, 0.5, 0.5] m | 3425 | $0.3\,\text{m} \leq h \leq 2\,\text{m}$ |

In Fig. 2, the set of obstacles that are part of the OA (e.g., working machines, storage areas, or static elements) and that add placement constraints to the sensors due to the occurrence of NLOS conditions are depicted.

In addition, a sensor placed on top of or in the immediate vicinity of machinery (e.g., aisles) may block the use of or access to it, so it is not permitted for sensors to be placed outside the walls of the industrial plant. The NLE contains all available positions for the possible placement of network elements. For this purpose, the space is divided through a grid-based method, in which the node location is restricted to grid locations. The spatial resolution used allows for decreasing the number of points analyzed and the time spent in the calculation of the sensor locations without significantly impacting the accuracy of the results [63].

In this sense, we define in Table II the spatial resolution used in each of the regions described above.

Hence, the industrial plant is stocked with machines and tools used to produce objects or services representing typical industrial conditions. The LPS deployed should interfere as little as possible in the course of a factory without altering his orography, it should avoid the placement of poles or other elements that hinder the elaboration of tasks, and should minimize the RMSE obtained at all locations. These restrictions require that each sensor that forms the proposed TDOA architecture must follow the following mathematical model [64]:

$$\max: Z = ff\left(ff_{\text{CRB}}, ff_{\text{pen}}\right) \tag{15}$$

$$\text{s.t.: } x_{\text{lim}_1} \leq x_i \leq x_{\text{lim}_2} \quad \forall x_i \in s_i; \quad s_i \in S; \; s_i \notin U \tag{16}$$

$$y_{\text{lim}_1} \leq y_i \leq y_{\text{lim}_2} \quad \forall y_i \in s_i; \; s_i \in S; \; s_i \notin U \tag{17}$$

$$z_{\text{lim}_1} \leq z_i \leq z_{\text{lim}_2} \quad \forall z_i \in s_i; \; s_i \in S; \; s_i \notin U \tag{18}$$

$$n_k, n'_k \geq n_{\min_{\text{TDOA}}} \quad \forall k \in K_{\text{TLE}} \tag{19}$$

$$n_k = \sum_{i=1}^{n_s} \text{cov}_{ki} \tag{20}$$

$$\text{cov}_{ki} = \begin{cases} 1, & \text{if } \text{SNR}_{ki} \geq \text{SNR}_{\text{threshold}_i} \\ 0, & \text{otherwise} \end{cases} \tag{21}$$

where $ff_{\text{CRB}}$ is a fitness function using the CRB error characterization of Section III; $ff_{\text{pen}}$ is a fitness function that use the penalizations for not attaining the restrictions of the optimization; $x_i$, $y_i$, and $z_i$ represent the spatial coordinates of a sensor $s_i$ of the TDOA architecture; $x_{\text{lim}_1}$, $y_{\text{lim}_1}$, and $z_{\text{lim}_1}$ are the lower bounds and $x_{\text{lim}_2}$, $y_{\text{lim}_2}$, and $z_{\text{lim}_2}$ are the upper bounds that define the region available for sensor placement in the space; $S$ is the set containing every potential NLE location for the architecture nodes having a subset $U$ that defines prohibited regions in space for LPS sensor placement (i.e., inside machinery or within walls); $n_k$ are the total number of effective sensors under coverage in a particular target location where a subset with a number of sensors $n'_k$ can be defined to optimally calculating the target position as defined in [64]; $n_{\min_{\text{TDOA}}}$ is the minimum set of sensors of the LPS architecture that allows the localization of the target placement (i.e., four sensors for 3-D localization, as shown in [65]); $K_{\text{TLE}}$ is the set of discretized points in the coverage area considered during the NLP optimization process [63]; $\text{cov}_{ki}$ indicates whether the sensor $i$ is in the coverage range of the point $k$ under consideration; $\text{SNR}_{ki}$ is a measure that evaluates the level of the signal with the level of the noise on the link from point $k$ to sensor $i$ and must be in the bounds of sensor sensitivity $i$ ($\text{SNR}_{\text{threshold}_i}$).

All these restrictions must be considered during the NLP optimization addressed in this article. However, this optimization must consider not only the general definition of the NLP but also some particular constraints derived from the scenario characteristics and the deployment of UWB localization systems in indoor spaces which recommends the disposition of the architecture sensors in the building walls [44], [66], [67]

$$x_i \equiv x_{\text{lim}_1} \Rightarrow y_{\text{lim}_1} \leq y_i \leq y_{\text{lim}_2} \tag{22}$$

$$x_i \equiv x_{\text{lim}_2} \Rightarrow y_{\text{lim}_1} \leq y_i \leq \rho \tag{23}$$

$$x_i \equiv \varsigma \Rightarrow \rho \leq y_i \leq y_{\text{lim}_2} \tag{24}$$

$$y_i \equiv y_{\text{lim}_1} \Rightarrow x_{\text{lim}_1} \leq x_i \leq x_{\text{lim}_2} \tag{25}$$

$$y_i \equiv y_{\text{lim}_2} \Rightarrow x_{\text{lim}_1} \leq x_i \leq \varsigma \tag{26}$$

$$y_i \equiv \rho \Rightarrow \varsigma \leq x_i \leq x_{\text{lim}_2} \tag{27}$$

$$L = \sum_{j=1}^{n_W} \Delta x_j + \Delta y_j \tag{28}$$

where $\rho$ and $\varsigma$ represent intermediate limits within the area available for sensor deployment, and $L$ is the total perimeter for a scenario with $n_W$ walls.

Fig. 3 shows the representation of the boundaries detailed in the formulas (22)–(28) defining the NLE space and identifying the walls that compose it.

The mathematical model presented above obtains an optimized combination of sensors for the NLP using the $ff_{\text{CRB}}$ and $ff_{\text{pen}}$

$$ff = c_1 \cdot ff_{\text{CRB}} - c_2 \cdot ff_{\text{pen}} \tag{29}$$

$$ff_{\text{CRB}} = \frac{1}{K_{\text{TLE}}} \sum_{k=1}^{K_{\text{TLE}}} \frac{\left(\text{RMSE}_{\text{ref}} - \text{RMSE}\left(S'_i(\text{AGV}_k)\right)\right)}{(\text{RMSE}_{\text{ref}})} \tag{30}$$

$$ff_{\text{pen}} = \frac{\sum_{i=1}^{N} R}{n_s} \tag{31}$$

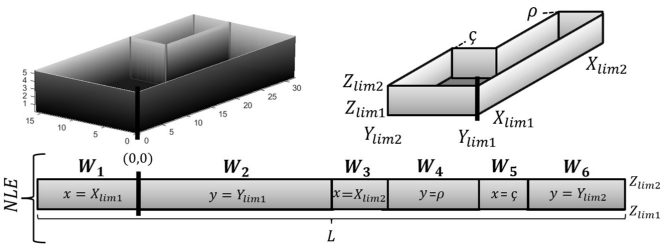


Fig. 3. Representation of the NLE region that composes the scenario.

where $c_1$ and $c_2$ are parameters for the weighting of each parameter; $S'_i$ is the subset of sensors obtaining the minimum localization uncertainty when calculating the target location over the available sensors at this point, as stated in [64]; $R$ is a penalty whose value is 0 for valid locations and 1 for forbidden ones, and $n_s$ is the number of sensors of the architecture.

Due to the high number of possibilities to be analyzed, the resolution of the problem (i.e., the points in NLE and TLE and sensors that compose the architecture), and the total number of possible valid combinations for the sensors in space, the NLP optimization addressed in this article cannot be solved in an adequate computational time if an exhaustive search were conducted. Therefore, the NLP is classified as NP-Hard, being usually solved through metaheuristic techniques [68].

## V. MA-VND-Chains

Mas are optimization techniques that combine concepts from two or more metaheuristics with the objective of overcoming some of their individual deficiencies [69] (e.g., local search (LS) and genetic algorithms (Gas) [70]). These types of algorithms are mostly population-based, where their individuals undergo individual learning through which they acquire a "cultural evolution," adding knowledge about the problem under study and improving the results obtained [70].

In addition, variations of the MAs have been introduced in the literature allowing a further adaptation to the characteristics of the problems in which they are being used. For example, the MA-SW-Chains employ the concept of LS chains so that, in one stage, the LS can continue the optimization of individuals where the previous invocation left off, using their achieved final parameter configurations [71]. Nevertheless, this algorithm is used to solve continuous problems, for this reason, we introduce the MA-VND-Chains variant for discrete problems such as the NLP addressed in this article [23]. The general performance of the applied technique is shown in Fig. 4.

First, during the initialization of the algorithm, the specific scenario of the industrial plant is encoded by incorporating the unique characteristics outlined in Section IV.

Second, as shown in Fig. 4, a number of potential solutions (i.e., the population) are randomly initialized and, subsequently subjected to evaluation (i.e., the fitness formulas (29)–(31) detailed in Section IV) to identify the best-adapted ones. When the LS criterion is not fulfilled, the convergence of the algorithm is checked. This step allows the algorithm to be executed as long as none of the stopping criteria, such as convergence or the maximum number of allowed iterations,

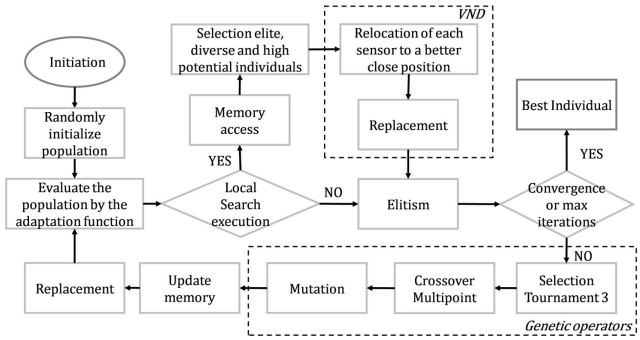


Fig. 4. Flowchart for MA-VND-Chains algorithm [23].

is met. Below, the individuals undergo modifications through selection, crossover, and mutation operators. This allows for generating new solutions with the objective of exploring the search space and for retaining the individuals that obtain the best results (i.e., the elitist operator).

However, when facing complex search scenarios, the possibility of obtaining high-quality solutions within certain regions (i.e., intensification) is reduced. Therefore, the subsequent generations have to evaluate criteria whether the predetermined performance criteria of the LS are satisfied. In this context, the LS allows performing a search within the solution space of an individual's neighborhood to find the locally optimal solution. To do so, the algorithm evaluates the neighborhood and selects the neighbor with the best fitness function to replace the current individual. Then, a new search is performed in the new neighborhood. This neighborhood change is performed deterministically through the variable neighborhood descent (VND) [23] algorithm. The LS algorithm continues until it obtains a local optimum or until it reaches a stopping criterion.

Nevertheless, not all individuals are selected for the LS. The choice of the individuals depends on the calculation of their improvement potential to reduce the convergence time of the algorithm. For this purpose, a memory stores where the number of times that each individual has not improved, the degree of improvement obtained by the individual in previous LS iterations, and the step used in the VND [23]. This memory is initialized at the beginning of the algorithm and undergoes changes whenever the individuals are modified (e.g., by the genetic operators or during the execution of the LS). Therefore, the benefits for each individual to undergo the LS process are calculated to reduce the number of possible executions without sacrificing the obtained accuracy [23].

As detailed in previous sections, the location of the sensors in the NLE of the industrial plant presents a large number of potential solutions, so the use of the MA-VND-Chains algorithm is very important to reduce time and improve the results. Each individual that is part of the population is a solution that obtains a higher or lower RMSE depending on its adaptation to the industrial plant.

In our previous research, these individuals were composed of the Cartesian coordinates (i.e., $x$, $y$, and $z$) representing the location of the sensors that make up the TDOA architecture [72]. Nevertheless, since the sensors are located on the building walls, this representation is not optimal for an industrial plant.

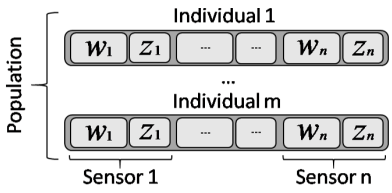


Fig. 5. Encoding used for the individuals of the population.

Fig. 5 shows the chromosome representation of the individuals. Two of the components of the reference system appear explicitly in the encoding and the third is reflected implicitly. Therefore, the value of $w_i$ allows us to know on which wall the sensor is located (i.e., $W_1, W_2, \ldots, W_6$), as shown in Fig. 3. In this representation of the NLE space, $w_i$ corresponds to the width coordinate of the sensor and $z_i$ is the height value. These parameters are the NLP decision variables, generating numerous potential locations.

This arrangement of the representation of the 3-D coordinates allows us to avoid generating invalid individuals outside the NLE. Thus, to carry out the decoding of the individual, it is necessary to apply the following constraints according to the dimensions of the NLE represented in Fig. 3:

$$W_{1,\min} \leq w_i \leq W_{1,\max} \Rightarrow (y_i = w_i) \wedge \left(x_i = x_{\lim_1}\right) \quad (32)$$

$$W_{2,\min} \leq w_i \leq W_{2,\max} \Rightarrow (x_i = w_i) \wedge \left(y_i = y_{\lim_1}\right) \quad (33)$$

$$W_{3,\min} \leq w_i \leq W_{3,\max} \Rightarrow (y_i = w_i) \wedge \left(x_i = x_{\lim_2}\right) \quad (34)$$

$$W_{4,\min} \leq w_i \leq W_{4,\max} \Rightarrow (x_i = w_i + \varsigma) \wedge (y_i = \rho) \quad (35)$$

$$W_{5,\min} \leq w_i \leq W_{5,\max} \Rightarrow (y_i = w_i + \rho) \wedge (x_i = \varsigma) \quad (36)$$

$$W_{6,\min} \leq w_i \leq W_{6,\max} \Rightarrow (x_i = w_i) \wedge \left(y_i = y_{\lim_2}\right) \quad (37)$$

where $w_i$ is the binary value encoded in the individual and corresponds to $x$ or $y$, and $W_{j,\min}$ and $W_{j,\max}$ corresponds to the limits of wall $j$, as shown in Fig. 3.

The encoding adopted allows homogenizing the $x$ and $y$ coordinates in $w$, generating valid positions in each crossover and mutation. In this sense, $w$ represents only the coordinate that is modified when advancing through each wall, while the other coordinate, which remains constant in this system, determines the wall at study.

The representation of the nodes without $w$ (i.e., the traditional $x$, $y$, and $z$ Cartesian coordinates used in our previous studies in rural and urban scenarios) generates a large number of invalid positions within the industrial plant, increasing the computational cost of the metaheuristic since there would be many more invalid positions than valid locations considering traditional encodings [72]. This modification has reduced the number of reachable solutions by more than 95%.

Section VI shows the deployed architectures obtained by the MA-VND-Chains algorithm as well as their RMSE calculated at each potential navigation position for the AGVs.

## VI. Results

This section shows the results of the optimization of the sensors' location for the UWB TDOA architecture deployed in the asymmetric 3-D environment presented in Section IV. This passive architecture does not require the synchronization

TABLE III
CONFIGURATION OF THE SYSTEM CLOCKS [58]

| Parameter | Magnitude | Unit |
|---|---|---|
| Clock frequency | 1 | GHz |
| Frequency-drift | U{-10, 10} | ppm |
| Initial-time offset | U{5, 6} | ns |
| Time from synchronization | 1 | $\mu s$ |
| Time-frequency product | 1 | |

TABLE IV
VALUES USED BY THE MA-VND-CHAINS SELECTED FOLLOWING THE METHODOLOGY PRESENTED IN [23] AND [73]

| | Parameter | Magnitude |
|---|---|---|
| Number of individuals | 80 | |
| Architectures | 11\9\7\5 sensors | |
| Stop Criteria | Generations | 120 |
| | Population Equal | 90% |
| Operators | Selection | Tournament 2 |
| | Crossover | Multipoint |
| | Mutation | 3% |
| | Elitism | 13% |
| LS | Frequency | 1/5 Generations |
| | Depth | 3 |
| | Individuals | 15% |
| Intensity | Threshold | 1 |
| | p | $\geq$0.07 m |
| Codification | Number of bits $w_i$ | 10 |
| | Number of bits $z_i$ | 6 |

between the TS clock and all the architecture sensors involved in the localization process since it uses relative times for the position calculation reducing the system complexity. However, the architecture sensors clocks may suffer deviations that disturb the time measurements, affecting the calculation of the AGV location. To minimize these uncertainties, as introduced in Section V, it is necessary to perform an adequate optimization of the sensors' location. Table III shows the selected characteristics for the anchors clocks of the proposed UWB TDOA architecture.

The architecture allows tracking single and multiple targets by calculating the difference in the arrival times of the signals on spatially separated receivers. However, in addition to clock errors, noise and signal degradation generate uncertainties in the range estimation although they are minimized by selecting the UWB signal characterization of Table I.

For these reasons, the MA-VND-Chains algorithm can select optimized positions for the sensors, reducing the positioning error of the AGVs within the TLE. The balance between exploration and intensification achieved allows us to optimally adapt to the orography and characteristics of the scenario. Table IV determines the tuning parameters for the MA-VND-Chains algorithm employed for the NLP optimization addressed. The algorithm has been coded in the MATLAB development environment and has been run on an Intel Core i9 CPU with 32 GB RAM.

As shown in Table IV, the MA-VND-Chains algorithm has been run for five, seven, nine, and 11 sensors TDOA configurations to compare the RMSE obtained by each WSN analyzed. The analysis of different distributions allows comparing the accuracy bounds provided by each of the TDOA architectures attained by the metaheuristic.

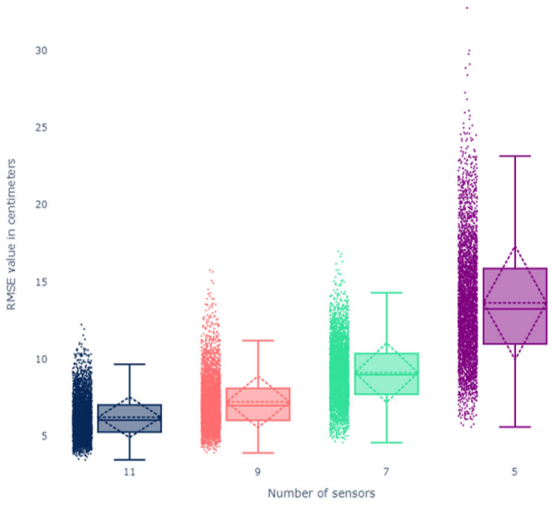


Fig. 6. RMSE distribution after the MA-VND-Chains optimization for 11, 9, 7, and 5 TDOA anchors, respectively. The error distributions highlight the media, typical deviation, median, interquartile ranges, and outlier values results obtained.

TABLE V
RMSE IN CENTIMETERS FOR THE MA-VND-CHAINS WITH FIVE, SEVEN, NINE, AND 11 SENSORS

| | 5 sensors | 7 sensors | 9 sensors | 11 sensors |
|---|---|---|---|---|
| Min | 5.58 | 4.57 | 3.90 | 3.45 |
| Mean | 13.64 | 9.11 | 7.21 | 6.21 |
| Max | 32.80 | 17.00 | 15.76 | 12.23 |
| Median | 13.24 | 8.97 | 6.97 | 6.02 |
| Std. Dev | 3.69 | 1.93 | 1.68 | 1.31 |
| $Q1$ | 10.96 | 7.71 | 6.00 | 5.24 |
| $Q3$ | 15.87 | 10.35 | 8.08 | 7.00 |
| Lower fence | 3.60 | 3.74 | 2.89 | 2.59 |
| Upper fence | 23.23 | 14.32 | 11.20 | 9.66 |

Thus, Fig. 6 and Table V present the error distribution achieved by each TDOA configuration examined.

Fig. 6 presents the error distributions obtained after analyzing the final architectures generated by the MA-VND-Chains algorithm. The left side of each element represents the error obtained for each point within the TLE (i.e., the potential locations for AGV navigation within the industrial scenario), without explicitly indicating their spatial coordinates. On the right side of Fig. 6, the boxplot provides a visual depiction of the statistical data for the error distributions.

As it can be seen in Table V, the five-sensor architecture presents a higher dispersion and a higher mean error value over the TLE, which prevents reaching adequate performance for AGV precision tasks such as pick and place, or the coordination with other industrial digitized devices which requires an error bound limited to 10 cm [74]. The rest of the architectures present an average error below 10 cm but the seven-sensor architecture presents a greater dispersion

than the nine-sensor and 11-sensor architecture, preventing the seven-sensor architecture to generate a robust, reliable, and stable localization system for AGVs navigation.

In the literature, there are studies that employ UWB technology combined with the TDOA architecture for target localization and tracking [75]. In this case [75], a four-sensor optimization methodology is implemented in a room with limited NLOS, approximately 7 × 5 m in size, resulting in an RMSE of 11.21 cm. Additionally, there are studies that replicate slightly larger environments to measure the positioning error. For instance, UWB MultiCell TDOA achieves an average error of 10 cm with eight sensors [76], or another UWB TDOA study that also analyzes multipath errors, obtains an average error of approximately 8 cm [77]. These errors are on the same order of magnitude as those observed in the previous table but it is important to highlight that our analyzed scenario is larger and more complex.

The differences between the nine- and 11-sensors distributions obtained in this article remain significant, but they are less pronounced compared to five- and seven-sensors distributions. This can be due to the fact that, in particular AGV locations, the consideration of a greater number of sensors to calculate the target location does not necessarily lead to a reduction of the localization uncertainties as demonstrated in [64]. However, the upper fence below 10 cm in the error distribution, the stability of the architecture under potential sensor failures [15], and the potential for the network to cover various tags at the same time (e.g., AGVs fleets [78]) recommends the deployment of the 11-sensor architecture in the industrial scenario proposed.

The study of architectures with a greater number of sensors was discarded since no significant difference in the error bounds can be achieved to justify the deployment of an architecture with higher costs and higher energy consumption. In addition, the theoretically achieved accuracy of 11-sensor architecture can even be increased through the treatment of the localization signal to partially mitigate NLOS and multipath effects following the research presented in Section II.

We also demonstrated in Section II the importance of performing a pre-deployment analysis of the network, since it reduces the uncertainty in the navigability area of the targets. Therefore, we have performed a comparison between an optimized architecture with a CRB without multipath ($CRB_{noise/clock}$) (i.e., the most complete actual literature model considering noise and clock uncertainties) and our proposal of this article that adds the multipath effect to the CRB ($CRB_{complete}$) (i.e., a model considering noise, clock and multipath uncertainties as introduced in Section III).

Subsequently, the two final sensor distributions achieved through the MA-VND-Chains algorithm presented in Section V (i.e., one optimization considering the $CRB_{noise/clock}$ and the other considering the $CRB_{complete}$ of this article) are evaluated through the CRB complete model in the factory introduced in Section IV.

Fig. 7 shows the shape, distribution, and most probable values of the error obtained for the two optimized LPSs using an 11-sensor UWB TDOA architecture. A higher density value

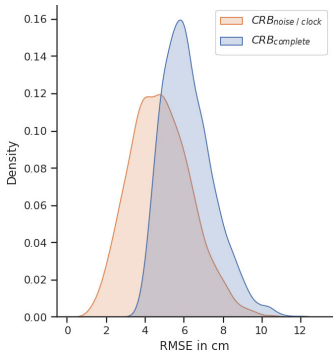


Fig. 7. RMSE distribution of the points that compose the TLE for two different optimized UWB TDOA architectures: 1) following an error model that considers noise and clock uncertainties in orange and 2) following an error model that considers noise, clock, and multipath uncertainties in blue.

indicates that more points in the TLE exhibit that RMSE value, signifying a more homogeneous error distribution.

The error difference perceived in Fig. 7 is with the differences presented in [28] between our previous CRB error model of [27] and the actual experimentation on an indoor UWB TDOA indoor system analyzed in [28]. In addition, the increased error due to the multipath interference effects is about 3 cm, which is around the reference values obtained in UWB experimentation [47] which further validates our novel CRB error model introduced for the first time in this article.

The multipath and the NLOS conditions are factors that degrade the signal emitted by the AGV, thus increasing the location uncertainty of the position calculation. It should be noted that these effects are increased when the number of obstacles is higher or with reflective surfaces, as frequently happens on the floor of the industrial plant (i.e., low area) due to the placement of machines, tools, and material.

So it is important to perform an exhaustive error analysis considering the different heights that autonomous mobile robots can have. Therefore, a classification considering the most common types of AGVs found in the factory is done.

The first category, called Low (i.e., 30–70 cm height) presents harsher conditions and refers to the area mainly occupied by AGVs such as Amazon Robotics' Kiva or Mobile Industrial Robots' MIR100. Medium height is for those robots such as Atlas Robotics with a height of less than 120 cm. Finally, the Maxi category includes larger AGVs such as those from Jungheinrich (i.e., less than 200 cm). The division allows us to analyze and compare the influence of LOS/NLOS and multipath conditions on the localization accuracy of AGVs of different heights.

Table VI shows the error measurements obtained by the optimized architecture deployed in the scenario for each of the different heights.

As shown in the previous Table, the optimized sensor configuration presents mean accuracy values that differ up to 4.14%, 0.33%, and 1.66% from the accuracy results presented over the low, medium, and maxi areas, respectively. These low variances in the error distributions of the three regions demonstrate the adequate performance of the metaheuristic for attaining a robust and balanced sensor arrangement that

TABLE VI
STATISTICAL RESULTS FOR THE RMSE FOR THE MA-VND-CHAINS WITH 11 ANCHORS ACCORDING TO THE DIFFERENT HEIGHT OF THE TLE

| | Low | Medium | Maxi | Total |
|---|---|---|---|---|
| Min | 3.50 | 3.72 | 3.45 | 3.45 |
| Mean | 6.46 | 6.20 | 6.09 | 6.21 |
| Max | 12.23 | 10.69 | 11.94 | 12.23 |
| Median | 6.28 | 6.00 | 5.92 | 6.02 |
| Std. Dev | 1.40 | 1.28 | 1.29 | 1.31 |
| Range | 8.73 | 6.96 | 8.49 | 8.78 |
| $Q1$ | 5.37 | 5.26 | 5.18 | 5.24 |
| $Q3$ | 7.33 | 7.02 | 6.82 | 7.00 |

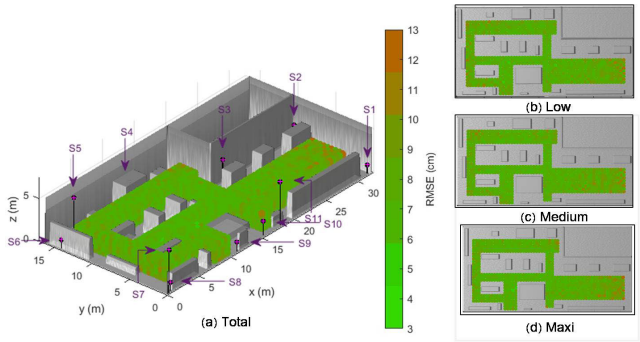


Fig. 8. RMSE evaluation in centimeters for each potential target location under the detailed scenario described in Section IV. (a) Represents the total points of TLE within the industrial plant. (b) Depicts the low range of TLE, covering target heights ranging from 30 to 70 cm. (c) Shows the medium range of TLE, encompassing targets at heights less than 120 cm. (d) Represents the maximum range of TLE, including targets with heights up to 200 cm. The spatial location for the final optimized sensor distribution of the UWB TDOA architecture deployed in this article is depicted in magenta.

minimizes the error throughout the entire TLE region guaranteeing the optimal performance of the localization architecture for any kind of industrial mobile robot.

Finally, Fig. 8 displays the RMSE evaluation for the optimized positioning architecture achieved using the MA-VND-Chains algorithm. The final LPS is deployed in the scenario, utilizing the predefined operating conditions as presented in this article. The figure serves as a comprehensive overview of the architecture performance, providing a visual representation of the quality of the positioning results.

## VII. CONCLUSION

The deployment of AGVs in industrial scenarios is opening a collaborative framework for internal transportation that increases the overall efficiency of factories. The embedded intelligence in these vehicles enables their autonomous navigation in the industrial plant. However, their localization system does not yet allow some precision tasks to be addressed by AGVs.

Consequently, we propose in this article the deployment of an ad hoc WSN based on UWB signal modulation for designing a robust and accurate localization system for the indoor precise navigation of AGVs.

UWB signal modulation takes advantage in these contexts of the very short duration of the pulses and of the large bandwidth to reduce multipath and NLOS negative effects on the localization signal thereby promoting the definition of a robust indoor localization system with centimeter accuracy.

However, the effective deployment of the proposed localization system requires an optimized location of the architecture nodes to minimize the error bounds of the architecture.

In this sense, we perform in this article an optimization of the sensors' location through the MA-VND-Chains metaheuristic. This optimization is guided by the minimization of the clock, noise, and multipath uncertainties of the localization system which are jointly modeled for the first time in the literature to the authors' knowledge.

Results have shown that an optimized 11-sensor architecture attains medium errors of 6 cm and an upper fence limited below 10 cm in the proposed industrial scenario, validating our proposed UWB TDOA localization system for AGVs' precise indoor navigation. In addition, the error distribution has shown stability for low, medium, and maxi-height AGVs which demonstrates the efficacy of the metaheuristic for reducing the localization errors in the entire navigation area thus designing a robust localization system for any type of industrial mobile robot within the factory.

Finally, the novel error model considering multipath has an error definition with actual UWB indoor experimentation also covering the differences of our previous CRB modeling considering noise and clock errors for actual deployments of UWB indoor localization systems. This constitutes a novel framework for determining the error bounds of an indoor localization architecture and for extracting valid conclusions that can maximize the theoretical performance of indoor localization systems enabling high-precision tasks in indoor spaces.

## REFERENCES

[1] V. Digani, L. Sabattini, C. Secchi, and C. Fantuzzi, "Ensemble coordination approach in multi-AGV systems applied to industrial warehouses," *IEEE Trans. Autom. Sci. Eng.*, vol. 12, no. 3, pp. 922–934, Jul. 2015.

[2] A. Martínez-Gutiérrez, J. Díez-González, R. Ferrero-Guillén, P. Verde, R. Álvarez, and H. Perez, "Digital twin for automatic transportation in industry 4.0," *Sensors*, vol. 21, no. 10, p. 3344, May 2021.

[3] L. Sabattini et al., "Technological roadmap to boost the introduction of AGVs in industrial applications," in *Proc. IEEE 9th Int. Conf. Intell. Comput. Commun. Process. (ICCP)*, Sep. 2013, pp. 203–208.

[4] S. Zhou, G. Cheng, Q. Meng, H. Lin, Z. Du, and F. Wang, "Development of multi-sensor information fusion and AGV navigation system," in *Proc. IEEE 4th Inf. Technol., Netw., Electron. Autom. Control Conf. (ITNEC)*, Jun. 2020, pp. 2043–2046.

[5] S. Bottigliero, D. Milanesio, M. Saccani, and R. Maggiora, "A low-cost indoor real-time locating system based on TDOA estimation of UWB pulse sequences," *IEEE Trans. Instrum. Meas.*, vol. 70, pp. 1–11, 2021.

[6] N. Petukhov, A. Chugunov, V. Zamolodchikov, D. Tsaregorodtsev, and I. Korogodin, "Synthesis and experimental accuracy assessment of Kalman filter algorithm for UWB ToA local positioning system," in *Proc. 3rd Int. Youth Conf. Radio Electron., Electr. Power Eng. (REEPE)*, Mar. 2021, pp. 1–4.

[7] K. W. Kolodziej and J. Hjelm, *Local Positioning Systems: LBS Applications and Services*. Boca Raton, FL, USA: CRC Press, 2017.

[8] W. Wang, Y. Zhang, and L. Tian, "TOA-based NLOS error mitigation algorithm for 3D indoor localization," *China Commun.*, vol. 17, no. 1, pp. 63–72, Jan. 2020.

[9] Y. Huang, S. Mazuelas, F. Ge, and Y. Shen, "Indoor localization system with NLOS mitigation based on self-training," *IEEE Trans. Mobile Comput.*, vol. 22, no. 7, pp. 3952–3966, Jul. 2022.

[10] R. Álvarez, J. Díez-González, N. Strisciuglio, and H. Perez, "Multi-objective optimization for asynchronous positioning systems based on a complete characterization of ranging errors in 3D complex environments," *IEEE Access*, vol. 8, pp. 43046–43056, 2020.

[11] X. Guo, N. Ansari, F. Hu, Y. Shao, N. R. Elikplim, and L. Li, "A survey on fusion-based indoor positioning," *IEEE Commun. Surveys Tuts.*, vol. 22, no. 1, pp. 566–594, 1st Quart., 2020.

[12] R. Álvarez, J. Díez-González, P. Verde, and H. Perez, "Comparative performance analysis of time local positioning architectures in NLOS urban scenarios," *IEEE Access*, vol. 8, pp. 225258–225271, 2020.

[13] J. Díez-Gonzalez, R. Álvarez, and H. Perez, "Optimized cost-effective node deployments in asynchronous time local positioning systems," *IEEE Access*, vol. 8, pp. 154671–154682, 2020.

[14] S. Hara, D. Anzai, T. Yabu, K. Lee, T. Derham, and R. Zemek, "A perturbation analysis on the performance of TOA and TDOA localization in mixed LOS/NLOS environments," *IEEE Trans. Commun.*, vol. 61, no. 2, pp. 679–689, Feb. 2013.

[15] J. Díez-González, R. Álvarez, N. Prieto-Fernández, and H. Perez, "Local wireless sensor networks positioning reliability under sensor failure," *Sensors*, vol. 20, no. 5, p. 1426, Mar. 2020.

[16] A. Savvides, H. Park, and M. B. Srivastava, "The $n$-hop multilateration primitive for node localization problems," *Mobile Netw. Appl.*, vol. 8, no. 4, pp. 443–451, 2003.

[17] N.-T. Nguyen and B.-H. Liu, "The mobile sensor deployment problem and the target coverage problem in mobile wireless sensor networks are NP-hard," *IEEE Syst. J.*, vol. 13, no. 2, pp. 1312–1315, Jun. 2019.

[18] B. Peng and L. Li, "An improved localization algorithm based on genetic algorithm in wireless sensor networks," *Cognit. Neurodynamics*, vol. 9, no. 2, pp. 249–256, Apr. 2015.

[19] J. Díez-González, P. Verde, R. Ferrero-Guillén, R. Álvarez, and H. Pérez, "Hybrid memetic algorithm for the node location problem in local positioning systems," *Sensors*, vol. 20, no. 19, p. 5475, Sep. 2020.

[20] J.-S. Pan, F. Fan, S.-C. Chu, Z. Du, and H. Zhao, "A node location method in wireless sensor networks based on a hybrid optimization algorithm," *Wireless Commun. Mobile Comput.*, vol. 2020, pp. 1–14, Oct. 2020.

[21] I. Strumberger, M. Minovic, M. Tuba, and N. Bacanin, "Performance of elephant herding optimization and tree growth algorithm adapted for node localization in wireless sensor networks," *Sensors*, vol. 19, no. 11, p. 2515, Jun. 2019.

[22] R. Rajakumar, J. Amudhavel, P. Dhavachelvan, and T. Vengattaraman, "GWO-LPWSN: Grey wolf optimization algorithm for node localization problem in wireless sensor networks," *J. Comput. Netw. Commun.*, vol. 2017, pp. 1–10, 2017.

[23] P. Verde, J. Díez-González, R. Ferrero-Guillén, A. Martínez-Gutiérrez, and H. Perez, "Memetic chains for improving the local wireless sensor networks localization in urban scenarios," *Sensors*, vol. 21, no. 7, p. 2458, Apr. 2021.

[24] R. Kaune, J. Hörst, and W. Koch, "Accuracy analysis for TDOA localization in sensor networks," in *Proc. 14th Int. Conf. Inf. Fusion*, 2011, pp. 1–8.

[25] A. Catovic and Z. Sahinoglu, "The Cramér–Rao bounds of hybrid TOA/RSS and TDOA/RSS location estimation schemes," *IEEE Commun. Lett.*, vol. 8, no. 10, pp. 626–628, Oct. 2004.

[26] B. Huang, L. Xie, and Z. Yang, "TDOA-based source localization with distance-dependent noises," *IEEE Trans. Wireless Commun.*, vol. 14, no. 1, pp. 468–480, Jan. 2015.

[27] R. álvarez, J. Díez-Gonzalez, L. Sánchez-González, and H. Perez, "Combined noise and clock CRLB error model for the optimization of node location in time positioning systems," *IEEE Access*, vol. 8, pp. 31910–31919, 2020.

[28] N. B. Torres, B. Etzlinger, E. Dehmollaian, and A. Springer, "Defining secure areas for TDOA-enhanced non-ideal distance bounding," in *Proc. Int. Wireless Commun. Mobile Comput. (IWCMC)*, 2022, pp. 348–353.

[29] R. Kunst, L. Avila, A. Binotto, E. Pignaton, S. Bampi, and J. Rochol, "Improving devices communication in industry 4.0 wireless networks," *Eng. Appl. Artif. Intell.*, vol. 83, pp. 1–12, Aug. 2019.

[30] P. J. Bora, Kishore, and P. C. Ramamurthy, "Polymer-metal/metal oxide-coated fly ash cenosphere composite film for electromagnetic interference shielding," in *Handbook of Fly Ash*, K. K. Kar, Ed. Oxford, U.K.: Butterworth-Heinemann, 2022, pp. 729–761.

[31] Z. Chen, C. Xu, C. Ma, W. Ren, and H.-M. Cheng, "Lightweight and flexible graphene foam composites for high-performance electromagnetic interference shielding," *Adv. Mater.*, vol. 25, no. 9, pp. 1296–1300, Mar. 2013.

[32] A. Courtay, M. L. Gentil, O. Berder, P. Scalart, S. Fontaine, and A. Carer, "Anchor selection algorithm for mobile indoor positioning using WSN with UWB radio," in *Proc. IEEE Sensors Appl. Symp. (SAS)*, Mar. 2019, pp. 1–5.

[33] W. Su, "Ultra wideband signals and systems in communication engineering (Ghavami, M. et al.; 2007) [book review]," *IEEE Signal Process. Mag.*, vol. 25, no. 5, pp. 122–123, Sep. 2008.

[34] S. Ullah, M. Ali, A. Hussain, and K. S. Kwak, "Applications of UWB technology," 2009, *arXiv:0911.1681*.

[35] G. Schroeer, "A real-time UWB multi-channel indoor positioning system for industrial scenarios," in *Proc. Int. Conf. Indoor Positioning Indoor Navigat. (IPIN)*, Sep. 2018, pp. 1–5.

[36] Y. Rahayu, T. A. Rahman, R. Ngah, and P. Hall, "Ultra wideband technology and its applications," in *Proc. 5th IFIP Int. Conf. Wireless Opt. Commun. Netw. (WOCN)*, 2008, pp. 1–5.

[37] J. Machaj, P. Brida, and S. Matuska, "Proposal for a localization system for an IoT ecosystem," *Electronics*, vol. 10, no. 23, p. 3016, Dec. 2021.

[38] S. Krishnan, R. X. M. Santos, E. Ranier Yap, and M. T. Zin, "Improving UWB based indoor positioning in industrial environments through machine learning," in *Proc. 15th Int. Conf. Control, Autom., Robot. Vis. (ICARCV)*, Nov. 2018, pp. 1484–1488.

[39] L. Barbieri, M. Brambilla, A. Trabattoni, S. Mervic, and M. Nicoli, "UWB localization in a smart factory: Augmentation methods and experimental assessment," *IEEE Trans. Instrum. Meas.*, vol. 70, pp. 1–18, 2021.

[40] X. Yang, "NLOS mitigation for UWB localization based on sparse pseudo-input Gaussian process," *IEEE Sensors J.*, vol. 18, no. 10, pp. 4311–4316, May 2018.

[41] Y. Cheng and T. Zhou, "UWB indoor positioning algorithm based on TDOA technology," in *Proc. 10th Int. Conf. Inf. Technol. Med. Educ. (ITME)*, Aug. 2019, pp. 777–782.

[42] Y. Liu, L. Yang, and J. Li, "Robust UWB indoor position tracking using TDOA measurements," in *Proc. IEEE 4th Int. Conf. Comput. Commun. (ICCC)*, Dec. 2018, pp. 736–743.

[43] M. Bocquet, C. Loyez, and A. Benlarbi-Delai, "Using enhanced-TDOA measurement for indoor positioning," *IEEE Microw. Wireless Compon. Lett.*, vol. 15, no. 10, pp. 612–614, Oct. 2005.

[44] H. Pan, X. Qi, M. Liu, and L. Liu, "Indoor scenario-based UWB anchor placement optimization method for indoor localization," *Exp. Syst. Appl.*, vol. 205, Nov. 2022, Art. no. 117723.

[45] C. Briso, C. Calvo, and Y. Xu, "UWB propagation measurements and modelling in large indoor environments," *IEEE Access*, vol. 7, pp. 41913–41920, 2019.

[46] F. Geyer and D. Schupke, "Precise onboard aircraft cabin localization using UWB and ML," 2022, *arXiv:2203.08403*.

[47] G. R. Opshaug and P. Enge, "GPS and UWB for indoor navigation," in *Proc. 14th Int. Tech. Meeting Satell. Division Inst. Navigat. (ION GPS)*, 2001, pp. 1427–1433.

[48] K. C. Ho and Y. T. Chan, "Solution and performance analysis of geolocation by TDOA," *IEEE Trans. Aerosp. Electron. Syst.*, vol. 29, no. 4, pp. 1311–1322, Oct. 1993.

[49] X. Chen, D. Wang, J. Yin, and Y. Wu, "Performance analysis and dimension-reduction Taylor series algorithms for locating multiple disjoint sources based on TDOA under synchronization clock bias," *IEEE Access*, vol. 6, pp. 48489–48509, 2018.

[50] P. Stoica and A. Nehorai, "MUSIC, maximum likelihood, and Cramér–Rao bound," *IEEE Trans. Acoust., Speech, Signal Process.*, vol. 37, no. 5, pp. 720–741, May 1989.

[51] J. Díez-González, R. Álvarez, P. Verde, R. Ferrero-Guillén, and H. Perez, "Analysis of reliable deployment of TDOA local positioning architectures," *Neurocomputing*, vol. 484, pp. 149–160, May 2022.

[52] M. Shalaby, M. Shokair, and N. W. Messiha, "Performance enhancement of TOA localized wireless sensor networks," *Wireless Pers. Commun.*, vol. 95, no. 4, pp. 4667–4679, Aug. 2017.

[53] A. Albaidhani and A. Alsudani, "Anchor selection by geometric dilution of precision for an indoor positioning system using ultra-wide band technology," *IET Wireless Sensor Syst.*, vol. 11, no. 1, pp. 22–31, Feb. 2021.

[54] R. Álvarez et al., "Accuracy analysis in sensor networks for asynchronous positioning methods," *Sensors*, vol. 19, no. 13, p. 3024, Jul. 2019.

[55] Z. Sahinoglu, S. Gezici, and I. Güvenc, *Ultra-wideband Positioning Systems: Theoretical Limits, Ranging Algorithms, and Protocols*. Cambridge, U.K.: Cambridge Univ. Press, 2008.

[56] T. S. Rappaport et al., *Wireless Communications: Principles and Practice*, vol. 2. Upper Saddle River, NJ, USA: Prentice-Hall, 1996.

[57] M. K. Elmezughi and T. J. Afullo, "An efficient approach of improving path loss models for future mobile networks in enclosed indoor environments," *IEEE Access*, vol. 9, pp. 110332–110345, 2021.
[58] J. Zhou, L. Shen, and Z. Sun, "A new method of D-TDOA time measurement based on RTT," in *Proc. MATEC Web Conf.*, vol. 207, 2018, p. 03018.
[59] M. Wang, Z. Chen, Z. Zhou, J. Fu, and H. Qiu, "Analysis of the applicability of dilution of precision in the base station configuration optimization of ultrawideband indoor TDOA positioning system," *IEEE Access*, vol. 8, pp. 225076–225087, 2020.
[60] A. A. M. Saleh and R. Valenzuela, "A statistical model for indoor multipath propagation," *IEEE J. Sel. Areas Commun.*, vol. SAC-5, no. 2, pp. 128–137, Feb. 1987.
[61] D. Ucinski, *Optimal Measurement Methods for Distributed Parameter System Identification*. Boca Raton, FL, USA: CRC Press, 2004.
[62] F. Domingo-Perez, J. Lazaro-Galilea, I. Bravo, A. Gardel, and D. Rodriguez, "Optimization of the coverage and accuracy of an indoor positioning system with a variable number of sensors," *Sensors*, vol. 16, no. 6, p. 934, Jun. 2016.
[63] A. Al-Qaisi, A. I. Alhasanat, A. Mesleh, B. S. Sharif, C. C. Tsimenidis, and J. A. Neasham, "Quantized lower bounds on grid-based localization algorithm for wireless sensor networks," *Ann. Telecommun.*, vol. 71, nos. 5–6, pp. 239–249, Jun. 2016.
[64] R. Álvarez, J. Díez-González, P. Verde, R. Ferrero-Guillén, and H. Perez, "Combined sensor selection and node location optimization for reducing the localization uncertainties in wireless sensor networks," *Ad Hoc Netw.*, vol. 139, Feb. 2023, Art. no. 103036.
[65] J. Díez-González, R. Álvarez, L. Sánchez-González, L. Fernández-Robles, H. Pérez, and M. Castejón-Limas, "3D TDOA problem solution with four receiving nodes," *Sensors*, vol. 19, no. 13, p. 2892, Jun. 2019.
[66] X. Yang, J. Wang, D. Song, B. Feng, and H. Ye, "A novel NLOS error compensation method based IMU for UWB indoor positioning system," *IEEE Sensors J.*, vol. 21, no. 9, pp. 11203–11212, May 2021.
[67] K. Szyc, M. Nikodem, and M. Zdunek, "Bluetooth low energy indoor localization for large industrial areas and limited infrastructure," *Ad Hoc Netw.*, vol. 139, Feb. 2023, Art. no. 103024.
[68] T. Hammerl, N. Musliu, and W. Schafhauser, "Metaheuristic algorithms and tree decomposition," in *Springer Handbook of Computational Intelligence*. Cham, Switzerland: Springer, 2015, pp. 1255–1270.
[69] W. E. Hart, N. Krasnogor, and J. E. Smith, *Recent Advances in Memetic Algorithms*. Berlin, Germany: Springer, 2004.
[70] R. Ferrero-Guillén, J. Díez-González, A. Martínez-Guitiérrez, and R. Álvarez, "Optimal COVID-19 adapted table disposition in hostelry for guaranteeing the social distance through memetic algorithms," *Appl. Sci.*, vol. 11, no. 11, p. 4957, May 2021.
[71] D. Molina, M. Lozano, C. García-Martínez, and F. Herrera, "Memetic algorithms for continuous optimisation based on local search chains," *Evol. Comput.*, vol. 18, no. 1, pp. 27–63, Mar. 2010.
[72] J. Díez-González, R. Álvarez, D. González-Bárcena, L. Sánchez-González, M. Castejón-Limas, and H. Perez, "Genetic algorithm approach to the 3D node localization in TDOA systems," *Sensors*, vol. 19, no. 18, p. 3880, Sep. 2019.
[73] R. Ferrero-Guillén, J. Díez-González, R. Álvarez, and H. Pérez, "Analysis of the genetic algorithm operators for the node location problem in local positioning systems," in *Proc. Int. Conf. Hybrid Artif. Intell. Syst.* Cham, Switzerland: Springer, 2020, pp. 273–283.
[74] K. Witrisal et al., "Chapter 9—Localization and tracking," in *Inclusive Radio Communications for 5G and Beyond*, C. Oestges and F. Quitin, Eds. New York, NY, USA: Academic, 2021, pp. 253–293.
[75] Y. Zhu, L. Huang, J. Liu, Z. Cao, J. Chen, and Z. Mu, "A real-time UWB location and tracking system based on TWR-TDOA estimation and a simplified MPGA layout optimization," *Mobile Inf. Syst.*, vol. 2022, pp. 1–10, Jul. 2022.
[76] G. Zhang, S. Krishnan, F. Chin, and C. C. Ko, "UWB multicell indoor localization experiment system with adaptive TDOA combination," in *Proc. IEEE 68th Veh. Technol. Conf.*, Sep. 2008, pp. 1–5.
[77] Y. Zhang and J. Zhao, "Indoor localization using time difference of arrival and time-hopping impulse radio," in *Proc. IEEE Int. Symp. Commun. Inf. Technol. (ISCIT)*, vol. 2, Dec. 2005, pp. 964–967.
[78] N. Singh, Q.-V. Dang, A. Akcay, I. Adan, and T. Martagan, "A matheuristic for AGV scheduling with battery constraints," *Eur. J. Oper. Res.*, vol. 298, no. 3, pp. 855–873, May 2022.

**Paula Verde** was born in León, Spain, in 1994. She received the B.S. degree in software engineering from the University of León, León, in 2016 and the M.S. degree in telecommunications from the University Oberta of Cataluña, Barcelona, Spain, in 2021. She is currently pursuing the Ph.D. degree with the University of León.

She is currently a Researcher with the Department of Mechanical, Computer, and Aerospace Engineering. She is working as an Instructor in the area of Computer Languages and Systems with the University of León. She received the grant for network programming, DEVNET from Cisco Networking Academy. Her research interests include communication networks, artificial intelligence, and localization.

**Javier Díez-González** was born in León, Spain, in 1994. He received the B.S. degree in aerospace engineering, the M.S. degree in aeronautical engineering, and the Ph.D. degree from the University of León, León, in 2016, 2018, and 2020, respectively, and the M.S. degree in artificial intelligence from the International University of Valencia, Valencia, Spain, in 2021.

He has followed the leadership program from the University Francisco de Vitoria, Madrid, Spain, where he graduated in 2017. He is currently a Researcher with the Department of Mechanical, Computer, and Aerospace Engineering, University of León, where he is working as a Lecturer in the area of mechanics. His research interests include high-performance localization, artificial intelligence, and industry 4.0.

**Rubén Álvarez** was born in León, Spain, in 1994. He received the B.S. degree in aerospace engineering from the University of León, León, in 2016, the M.S. degree in aeronautical engineering from the University of Leon, Leon, in 2018, the M.S. degree in artificial intelligence from the International University of Valencia, Valencia, Spain, in 2019, and the Ph.D. degree from the University of León, in 2020.

He started his Professional Career Leading with the Innovation Group of Natural Language Processing, Taiger Company also extending his collaboration with the Department of Mechanical, Computer, and Aerospace Engineering, University of León.

**Hilde Perez** received the B.E. degree in electrical and electronics engineering from the University of León, Leon, Spain, and the B.E. degree in mechanical engineering from the University of Oviedo, Oviedo, Spain, and the Ph.D. degree from the Polytechnic University of Madrid, Madrid, Spain, in 1990, 2004, and 2012, respectively.

She is a Full Professor and the Head of the Department of Mechanical, Computer, and Aerospace Engineering with the University of León. She has involved in different national research projects in collaboration with the Polytechnic University of Madrid. The research areas of interests are related to Industry 4.0, smart systems for manufacturing, automated guided vehicles, localization, and collaborative robots.